Supporting Information for

The Topmost Water Structure at a Charged Silica/Aqueous Interface Revealed by Heterodyne-Detected Vibrational Sum Frequency Generation Spectroscopy

Shu-hei Urashima,[†1] Anton Myalitsin, [‡1] Satoshi Nihonyanagi,[1,2] Tahei Tahara[1,2]*

[1] Molecular Spectroscopy Laboratory, RIKEN, 2-1 Hirosawa, Wako, Saitama 351-0198, Japan

[2] Ultrafast Spectroscopy Research Team, RIKEN Center for Advanced Photonics (RAP), 2-1 Hirosawa, Wako, Saitama 351-0198, Japan.

Present addresses

[†]Research Institute for Science & Technology, Tokyo University of Science, 2641 Yamazaki, Noda, Chiba 278-8510, Japan.

[‡]Function Analysis Department, NISSAN ARC Ltd., 1 Natsushima-cho, Yokosuka, Kanagawa 237-0061, Japan.

Corresponding Author

Corresponding Author: tahei@riken.jp

1. Experimental

Sample preparation: The silica sample used was a 3-mm thick plate of IR-grade fused silica purchased from Pier Optics. While we used a few substrates through the period of this study (months), neither substrate dependence nor long-term change of the spectra was recognized. The silica samples were cleaned by concentrated sulfuric acid (>10 hr) and thoroughly rinsed by copious amount of running water prior to use. To get dry and clean surface of the silica, the silica plate was blow-dried by nitrogen gas in a clean room (Class 5 (JIS B9920)). The cleanliness of the silica was confirmed by absence of any CH stretch bands in the $\chi^{(2)}$ spectrum. A 150-nm thick gold film with 8-angstrom titanium adhesion layer was prepared on about half area of the silica surface by electron-beam evaporation for reference measurements. The solutions used were prepared with milli-Q water, or HOD-D_2O which was made by mixing milli-Q water and D_2O (Kanto Chemical, 99.8 %D) with volume ratio of 1 : 4. The ionic strength of the solution was controlled by the addition of NaCl (Alfa Aesar, 99.99 %), whereas pH was adjusted to 12.0 ± 0.2 or 11.8 ± 0.1 (for H_2O or HOD-D_2O solution, respectively) by adding adequate amount of 1 M NaOH (Junsei, 97.0 %) dissolved in the corresponding waters. The pH value was measured by a pH meter (Horiba, B-212). For the HOD-D_2O solution, although we used the term "pH" without special attention for D^+ (or "pD") in this paper, we multiplied a factor of 0.943 to the pH meter reading then added 0.3 for the isotopic correction.[1-3] The same concentrations of NaOH and NaCl were used for H_2O and HOD-D_2O solutions.

HD-VSFG spectroscopy: The experimental setup of HD-VSFG spectroscopy has been described elsewhere.[1, 4] Briefly, the output of a regenerative amplifier (Spectra Physics, SpitfireProXP, 3.5 W, 1 kHz) was split into two to obtain a narrow-band visible pulse (ω_1) and a broadband infrared (IR) pulse (ω_2). A bandpass filter (Optoscience) was used to narrow the

bandwidth of ω_1 (center frequency: 795nm, bandwidth: 1.5 nm, *i.e.* 25 cm^{-1}, in full-width of half-maximum). The broadband IR pulse was generated by an optical parametric amplifier combined with a difference-frequency generation crystal (Spectra Physics, TOPAS C & DFG1). The ω_1 and ω_2 pulses were focused into a thin plate of y-cut quartz to generate sum-frequency (SF) used as a local-oscillator (LO). Then, the transmitted three pulses of ω_1, ω_2, and LO were again focused on the "buried" silica interface, after the LO passed through a 2-mm thick glass plate to be delayed. To compensate the delay between ω_1 and ω_2 which is generated while they pass in the sample silica substrate, a 0.2-mm thick glass plate was inserted to the ω_1 path between the y-cut quartz and the sample. The SF generated from the silica/aqueous interface and LO reflected at the same interface were introduced into a polychromator (HORIBA, HR 320) and were detected by a liquid nitrogen-cooled CCD (Princeton Instruments, Spec-10). The polarizations of the SF, ω_1, and ω_2 were set at s-, s-, and p-polarization, respectively (SSP polarization combination). The $\chi^{(2)}$ spectra of the silica/aqueous interface were normalized with that of the silica/gold interface, and the complex phase of the silica/gold interface was calibrated by using the $\chi^{(2)}$ spectrum of the dry silica/air interface as the phase standard. For this silica/air measurements, a small amount of D_2O was placed under the silica to substitute all the hydrogen atoms of surface silanol and adsorbed water into deuterium atoms.[1] Thus, this silica/air interface is non-resonant in the IR range examined, and hence the complex phase of $\chi^{(2)}$ can be considered zero (Previously, we have demonstrated that the complex phase of non-resonant $\chi^{(2)}$ signal at the air/silica interface is negative real (180 degree). Therefore, the phase of non-resonant $\chi^{(2)}$ signal at the silica/air interface, which is upside down, is positive real (0 degree).).[1, 5] To verify that our results and conclusion are not affected by the potential phase error, we calculated $Im\chi^{(2)}$ spectra with phases intentionally rotated by ± 10 degrees and confirmed that the essential features of the

spectra in fact remained unchanged. At the very high salt concentration used in the present study, the refractive index of the solution is not constant when the salt concentration is changed, and it affects the reflectivity of LO. The spectra shown in this paper have been corrected for the reflectivity as well as the Fresnel factor. The details of this correction procedure are described later (section 5 in this SI).

2. Intensity of the $\chi^{(2)}_{\mathrm{total}}$ with respect to the surface potential

In this section, we describe the relation between the surface potential and the spectral intensity of the $\chi^{(2)}_{\mathrm{total}}$ (*i.e.*, eq. 1 in the main text). Because the observed $\chi^{(2)}$ spectrum $\left(\chi^{(2)}_{\mathrm{total}}\right)$ can be decomposed into $\chi^{(2)}_{\mathrm{top}}$ and $\chi^{(2)}_{\mathrm{EDL}}$, $\chi^{(2)}_{\mathrm{total}}$ can be represented as,[6-8]

$$\chi^{(2)}_{\mathrm{total}} = \chi^{(2)}_{\mathrm{top}} + \chi^{(2)}_{\mathrm{EDL}} = \chi^{(2)}_{\mathrm{top}} + \int_0^{\infty} \chi^{(2)}_{\mathrm{B}} \mathrm{e}^{i\Delta k_z z} E(z) dz \,. \qquad \text{(S1)}$$

Here, $\chi^{(2)}_{\mathrm{B}}$ is the $\chi^{(2)}$ response of the water in EDL per unit electric field $[E(z)]$, which mainly arises from the orientation of water induced by the electric field in the EDL.[9] Δk_z and z are inverse of coherence length and the distance from the surface, respectively, and $\mathrm{e}^{i\Delta k_z z}$ describes the phase-mismatch of the reflected SFG generated at the different depth in the EDL.[6] For the ionic strength examined in this study ($\geq$ 0.01 M), because the electric field $E(z)$ decays within a few nanometers (see Figure S1b in the next section), the phase mismatch term $\mathrm{e}^{i\Delta k_z z}$ in this equation is negligible.[1] Therefore, the equation can be simplified as

$$\chi^{(2)}_{\mathrm{total}} = \chi^{(2)}_{\mathrm{top}} + \chi^{(2)}_{\mathrm{B}} \int_0^{\infty} E(z) dz = \chi^{(2)}_{\mathrm{top}} + \chi^{(2)}_{\mathrm{B}} \phi_0 \quad , \qquad \text{(S2)}$$

where $\phi_0 = \int_0^{\infty} E(z) dz$ is the surface potential. This equation indicates that the observed $\chi^{(2)}_{\mathrm{total}}$ intensity is linear to the surface potential if $\chi^{(2)}_{\mathrm{top}}$ spectrum is independent of the ionic strength.

3. Electric double layer properties calculated by the modified Poisson-Boltzmann theory: Electric potential, electric field, and local concentration of hydrated ions

In this section, we describe calculation of the properties of the electric double layer, *i.e.*, electric potential, electric field, and local concentration of hydrated ions, using the modified Poisson-Boltzmann theory.[6, 10]

The modified Poisson-Boltzmann theory is a mean-field model to describe the electric field and the electric potential in the Gouy-Chapman layer, based on the Poisson-Boltzmann equation:

$$\rho(\mathrm{z}) = -\varepsilon\varepsilon_0 \frac{\mathrm{d}^2\phi(z)}{\mathrm{d}z^2} \quad , \tag{S3}$$

where $\rho(z)$, ε, ε_0, and ϕ are the local charge density, relative dielectric constant, dielectric constant in vacuum, and the electric potential, respectively. While the traditional Poisson-Boltzmann theory treats ions as point charge, the modified Poisson-Boltzmann theory takes account of finite ion-size effect. This modification enables the theory to describe saturation of the local ion concentration. The local ion concentration is given by modified Poisson-Boltzmann theory as:

$$n_{\pm} = \frac{n_0 \exp\left(\mp \frac{me\phi}{k_{\mathrm{B}}T}\right)}{1 + 2\nu \sinh^2\left(\frac{me\phi}{2k_{\mathrm{B}}T}\right)} \quad , \tag{S4}$$

where n_+ and n_- are the local ion concentration (number density) of cation and anion, respectively. n_0, k_{B}, T, m, and e are the ion concentration in the bulk, the Boltzmann constant, the absolute temperature, the ionic valence, and the elementary charge, respectively. ν is the parameter to introduce the finite-ion size effect, which is defined as:

$$\nu = 2a^3 n_0 \quad , \tag{S5}$$

where a is the "ion size" including the hydration shell. This means that the volume of one hydrated cation (V) is represented as $V = a^3$, and hence the maximum concentration ($n_{\max}$), at which the hydrated cations are packed without any vacant space, is described as $n_{\max} = V^{-1} = a^{-3}$. Thus, the parameter ν is represented also as $\nu = 2n_0/n_{\max}$, which is considered as the mean volume fraction of ions in the bulk. For negatively charged interfaces, the potential ϕ is given as:

$$\phi_0 \equiv \phi(0) = -\frac{2k_{\mathrm{B}}T}{me}\sinh^{-1}\left\{\sqrt{\frac{1}{2\nu}\left[\exp\left(\frac{\sigma^2\nu}{4n_0\varepsilon\varepsilon_0 k_{\mathrm{B}}T}\right)-1\right]}\right\} \quad , \tag{S6}$$

and

$$\frac{d\phi(z)}{dz} = \frac{2men_0\lambda_{\mathrm{D}}}{\varepsilon\varepsilon_0}\sqrt{\frac{2}{\nu}\ln\left[1+2\nu\sinh^2\left(\frac{me\phi}{2k_{\mathrm{B}}T}\right)\right]} \quad , \tag{S7}$$

where $\lambda_{\mathrm{D}} = \sqrt{\frac{\varepsilon\varepsilon_0 k_{\mathrm{B}}T}{2m^2e^2n_0}}$ is the Debye length, which represents the thickness of the Gouy-Chapman layer calculated with the traditional Poisson-Boltzmann theory. σ is the surface charge density in dimension of C/m^2.

To calculate the surface potential ϕ_0 by eq. S6, the "ion size" a and the surface charge density σ are required. From refs. 6 and 7, we adopted $a = 7$ [Å] and $\sigma = 0.87e$ [C/nm^2], respectively. Note that the surface charge density σ is still under debate,[7, 11] and this surface charge of $0.87e$ was the one determined for the planar silica/water interface by second harmonic generation measurements.[7] We also need the dielectric constant ε, which depends on the ion concentration. Because the local ion concentration in the Gouy-Chapman layer varies with the distance from the surface, the dielectric constant in the Gouy-Chapman layer was estimated as follows. First, the dielectric constant of the bulk NaCl solution was taken from literature.[12-13] For

bulk solutions, it was reported that sodium ions contribute to the change of the dielectric constant than chloride ions, and that the relative contribution is Na^+ : Cl^- = 8 : 3.[12, 14] Thus, we describe the dielectric constant ε in the EDL as

$$\varepsilon = \varepsilon_{\mathrm{w}} - \frac{1}{11}[8\Delta\varepsilon(n_+) + 3\Delta\varepsilon(n_-)] \quad , \tag{S8}$$

where $\varepsilon_{\mathrm{w}} = 78.36$ is the dielectric constant of neat water, and $\Delta\varepsilon(n)$ is the difference of the dielectric constant of neat water and that of NaCl solution[12] having ionic strength of n. Because ϕ, $n_{\pm}$, and ε are related with each other, they were numerically determined to be self-consistent through iteration of the calculation.

The obtained electric potential ϕ, the electric field $E = -\frac{\mathrm{d}}{\mathrm{d}z}\phi$, and the local cation concentration n_+ are summarized in Figure S1. Interestingly, in the range of the bulk ionic strength of 0.01-1 M, the calculated electric field E and cation concentration n_+ at the topmost region (ca. z < 3 angstrom) are almost independent from the bulk ionic strength, although the surface potential ϕ_0 is highly dependent on the bulk ionic strength. This result is consistent with our conclusion that the increase of the bulk ionic strength only gives rise to the decrease of the $\chi^{(2)}_{\mathrm{EDL}}$ component in the ionic strength range of 0.01-2 M. On the other hand, at the bulk ionic strength higher than 2 M, the cation concentration n_+ in the topmost region shows significant increase with the bulk concentration while the surface potential ϕ_0 is more or less saturated. This also accords with our argument that the topmost water structure in very high ionic strength range (> 2 M) varies from that at lower ionic strength.

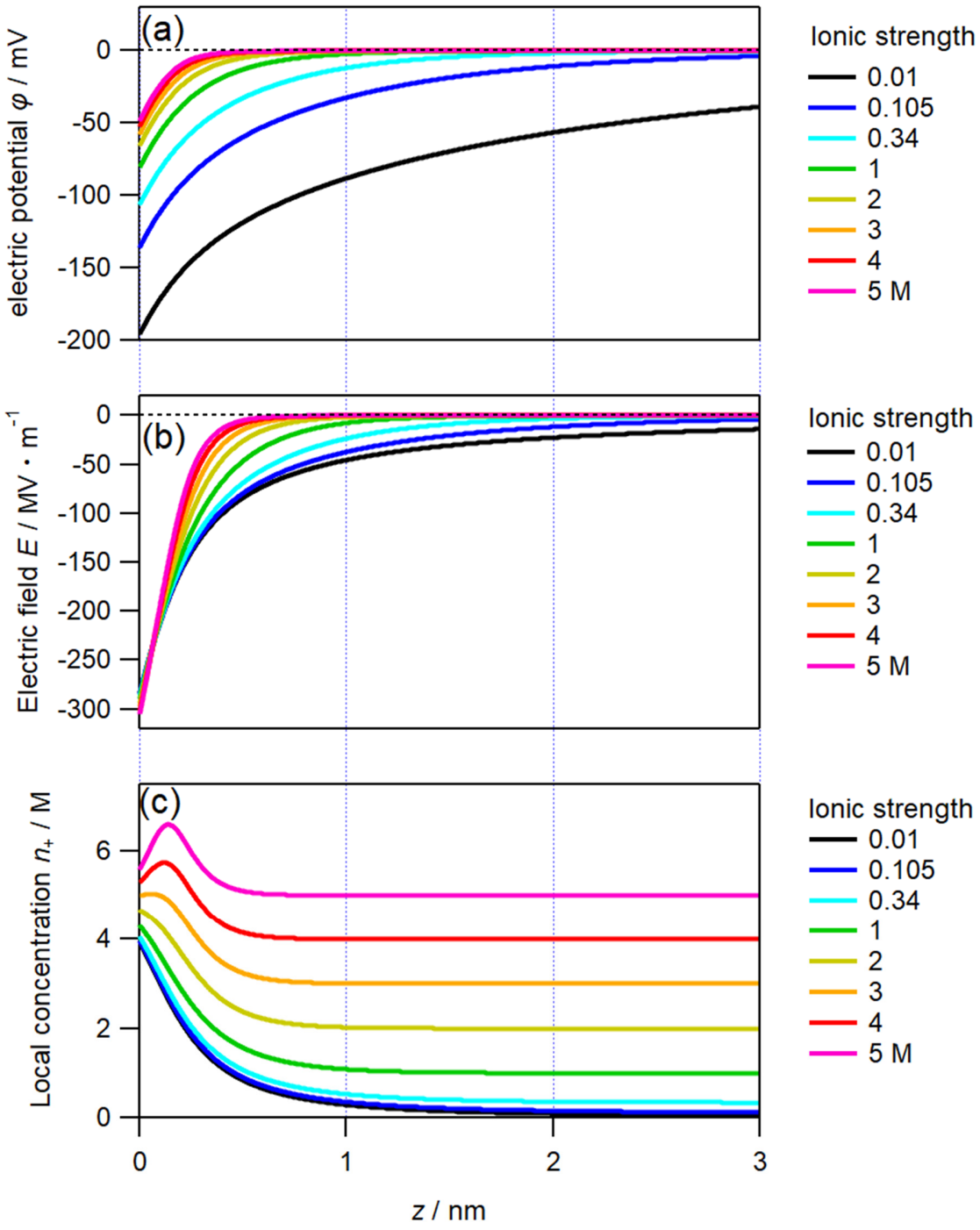

Figure S1. Electric double layer properties obtained by the modified Poisson-Boltzmann theory. (a) The electric potential ϕ obtained by numerical integration using eqs. S4-S8. (b) The electric field E obtained by numerical differentiation of ϕ. (c) The local concentration of the hydrated cation (n_+) near the surface, obtained by eq. S4.

4. Im$\chi^{(2)}$ spectra measured with HOD-D_2O solution

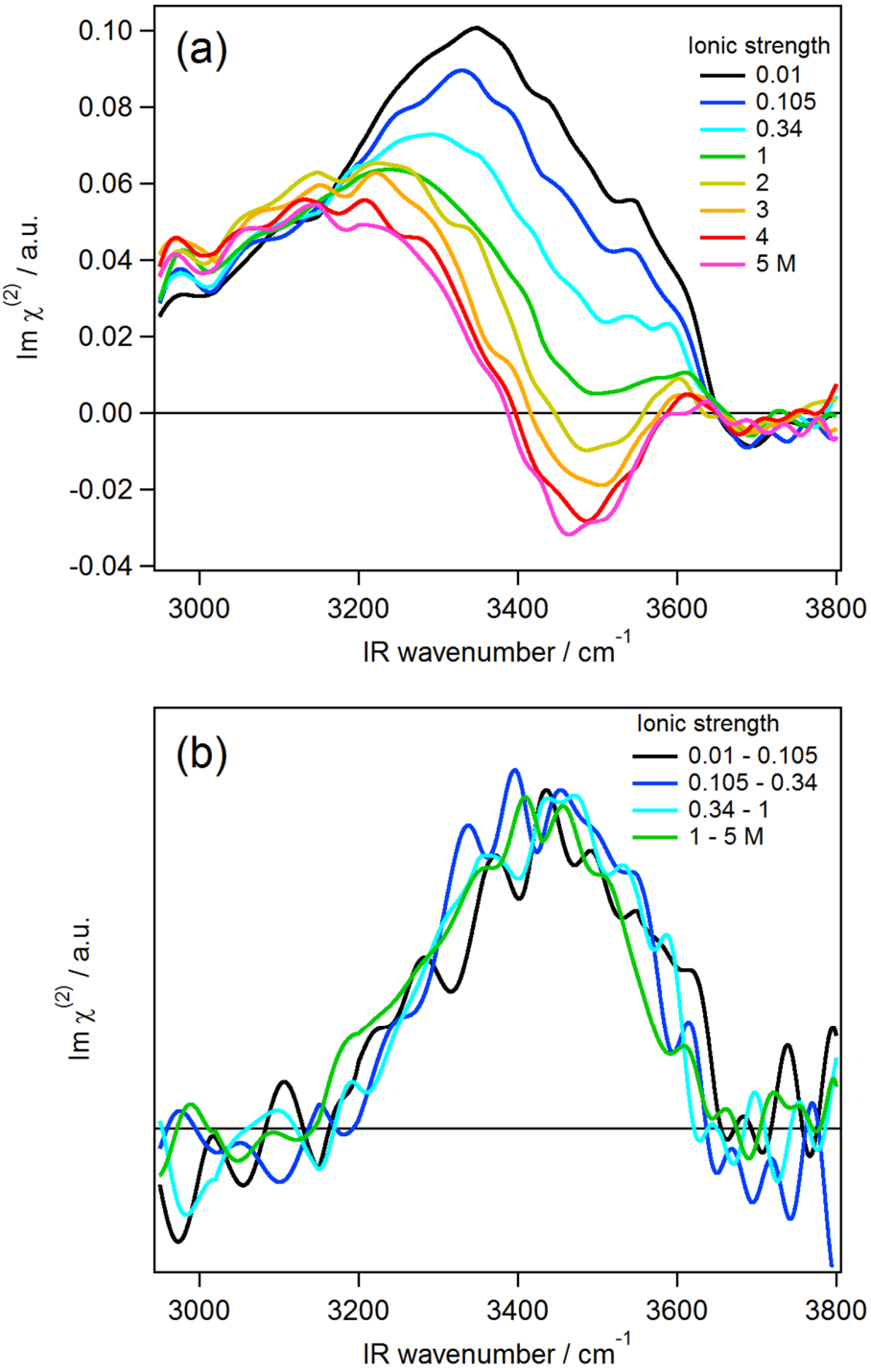

Figure S2. (a) Im$\chi^{(2)}$ spectra of silica/HOD-D_2O aqueous interfaces at pH 12 with ionic strength from 0.01 to 5 M. (b) The area-normalized difference spectra.

5. Fresnel and reflectivity correction

All the spectra shown in this paper have been corrected for the Fresnel factor and reflectivity which depend on the ionic strength. In this section, we describe this correction procedure in detail.

Because the detected light is the sum of the sum-frequency (SF) from the sample and the local oscillator (LO) reflected at the interface, the total intensity of the probed light is described as:

$$I_{\mathrm{probe}} = \left|E_{\mathrm{sam}} + RE_{\mathrm{LO}}e^{i\omega T}\right|^2 = |E_{\mathrm{sam}}|^2 + |RE_{\mathrm{LO}}|^2 + E_{\mathrm{sam}}R^*E_{\mathrm{LO}}e^{-i\omega T} + E_{\mathrm{sam}}^*RE_{\mathrm{LO}}e^{+i\omega T} \quad , \text{(S9)}$$

where E_{sam} and E_{LO} are the electric field of the sample SF and the LO, R is the Fresnel reflection coefficient of LO at the interface, and T is the delay between the sample SF and the LO. By picking up the $E_{\mathrm{sam}}R^*E_{\mathrm{LO}}e^{-i\omega T}$ term[4] and comparing it with that of the reference measurement, we obtain

$$\chi_{\mathrm{exp}}^{(2)} = \frac{R^*\chi_{\mathrm{eff,sam}}^{(2)}}{R_{\mathrm{ref}}^*\chi_{\mathrm{eff,ref}}^{(2)}} \quad , \text{(S10)}$$

where $\chi_{\mathrm{eff,sam}}^{(2)}$, $\chi_{\mathrm{eff,ref}}^{(2)}$, and R_{ref} are the effective second-order susceptibility at the sample and reference interfaces and the reflection coefficient of LO at the reference interface, respectively.

For SSP polarization combination used in the present study, the effective second-order susceptibility is described as

$$\chi_{\mathrm{eff,SSP}}^{(2)} = L_{3Y}L_{1Y}L_{2Z}\sin\theta_{2\mathrm{r}}\,\chi_{YYZ}^{(2)} \quad , \text{(S11)}$$

where $L_{3Y}L_{1Y}L_{2Z}$ is the Fresnel factor, $\theta_{2\mathrm{r}}$ is the reflection angle of ω_2 (IR) beam, and $\chi_{YYZ}^{(2)}$ is the corresponding tensor element of the second-order susceptibility of the interface. The Fresnel factor is given[15] as

$$L_{3Y} = \frac{2n_{\mathrm{a3}} \cos\theta_{3\mathrm{r}}}{n_{\mathrm{a3}} \cos\theta_{3\mathrm{r}} + n_{\mathrm{b3}} \cos\theta_{3\mathrm{t}}}$$

$$L_{1Y} = \frac{2n_{\mathrm{a1}} \cos\theta_{1\mathrm{r}}}{n_{\mathrm{a1}} \cos\theta_{1\mathrm{r}} + n_{\mathrm{b1}} \cos\theta_{1\mathrm{t}}} \tag{S12}$$

$$L_{2Z} = \frac{2n_{\mathrm{b2}} \cos\theta_{2\mathrm{r}}}{n_{\mathrm{a2}} \cos\theta_{2\mathrm{t}} + n_{\mathrm{b2}} \cos\theta_{2\mathrm{r}}} \left(\frac{n_{\mathrm{a2}}}{n_2'}\right)^2$$

with

$$n_2' = \sqrt{\frac{n_{\mathrm{a}}^2 + n_{\mathrm{b}}^2 + 4}{2(n_{\mathrm{a2}}^{-2} + n_{\mathrm{b2}}^{-2} + 1)}} \quad , \tag{S13}$$

where $n_{\mathrm{a}i}$ and $n_{\mathrm{b}i}$ are the refractive indices of medium a (silica) and b (solution) at the frequency of ω_i, and $\theta_{i\mathrm{r}}$ and $\theta_{i\mathrm{t}}$ are the reflection and transmission angle of ω_i beam, respectively. n_2' is the refractive index of the interface, which is defined as first proposed by Shen *et al*. [15]

Combining eqs. S10 and S11, the experimentally observed spectrum, $\chi_{\mathrm{exp}}^{(2)}$, is represented as:

$$\chi_{\mathrm{exp}}^{(2)} \propto R^* L_{3Y} L_{1Y} L_{2Z} \chi_{YYZ}^{(2)} \quad . \tag{S14}$$

Therefore, for comparing the spectra measured with various ionic strengths (which lead to different refractive indices), we need to divide the experimentally observed spectra by the factor of $R^* L_{3Y} L_{1Y} L_{2Z}$. The refractive indices were taken from several references.[16-20] Because the literature does not cover all the conditions of our measurements, we interpolated the refractive index given in the literature, especially in the infrared region. The term $L_{3Y} L_{1Y} L_{2Z}$ is insensitive to the ionic strength: only about 5 % change by addition of 5 M NaCl. In contrast, the reflection coefficient R^* is sensitive to the change of the ionic strength. For the calculation of R^* (the reflection coefficient of visible light at ~630 nm), we assume that the refractive indices of NaCl

solution in HOD-D_2O are the same as those of H_2O in the visible region. The calculated total correction factors, $R^*L_{3Y}L_{1Y}L_{2Z}$, for H_2O solutions are shown in Figure S3.

To confirm the reliability of the correction, we compared the corrected $|\chi^{(2)}|^2$ spectra with homodyne-detected spectra at high ionic strength. This is because the homodyne-detected spectra are measured without the LO so that they are not affected by the reflectivity R^*. The corrected $|\chi^{(2)}|^2$ spectra for the H_2O solutions are well overlapped with the homodyne spectra as shown in the left panels of Figure S4. For HOD-D_2O solutions, however, the same correction method somehow failed to reproduce the homodyne spectra. Therefore, we experimentally determined the reflectivity $|R|^2$ at the silica/HOD-D_2O solution interfaces using the SFG signal obtained in the region of $\omega_2 > 3750$ cm^{-1}, where the SFG from this interface is negligibly weak so that the observed SFG signal is considered to arise solely from the LO reflected at the silica interface. The $|\chi^{(2)}|^2$ spectra corrected with this reflectivity reasonably reproduced the homodyne spectra as shown in the right panels of Figure S4, and hence this correction was used for discussion on the silica/HOD-D_2O solution interfaces.

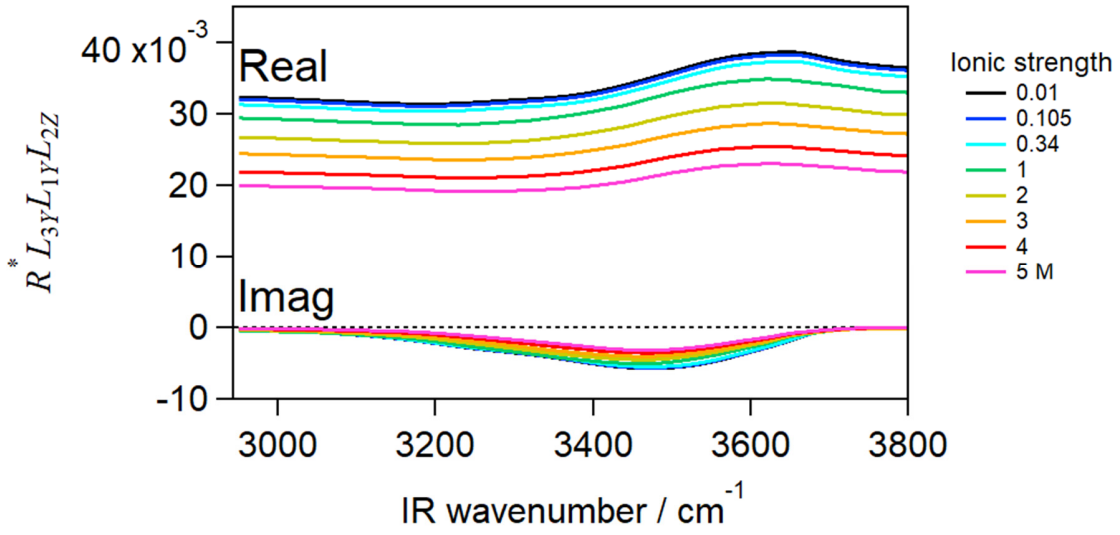

Figure S3. The $R^*L_{3Y}L_{1Y}L_{2Z}$ components calculated at various NaCl concentration in H_2O.

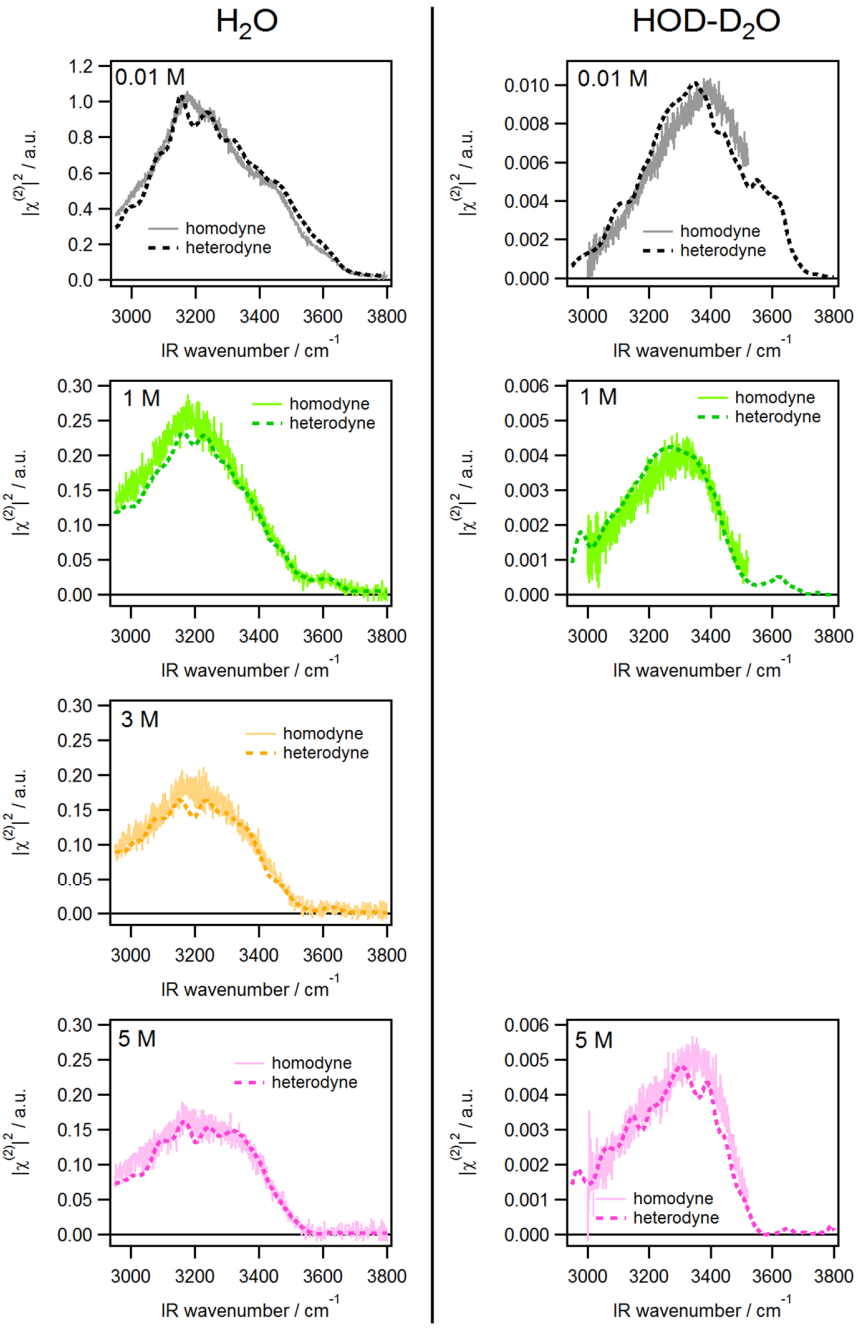

Figure S4. Comparison of $\left|\chi^{(2)}\right|^2$ spectra reconstructed from the complex $\chi^{(2)}$ spectra (broken lines) and those directly measured by homodyne-detected VSFG measurements (solid lines). Left: H_2O, right: HOD-D_2O solution. Ionic strength for each measurement is given in the figure. Fresnel correction ($L_{3Y}L_{1Y}L_{2Z}$ derived from eq. S12) is applied for both of homodyne- and heterodyne-detected spectra. The reflectivity correction is applied only to the heterodyne-detected spectra.

6. $|\chi^{(2)}|^2$ spectra

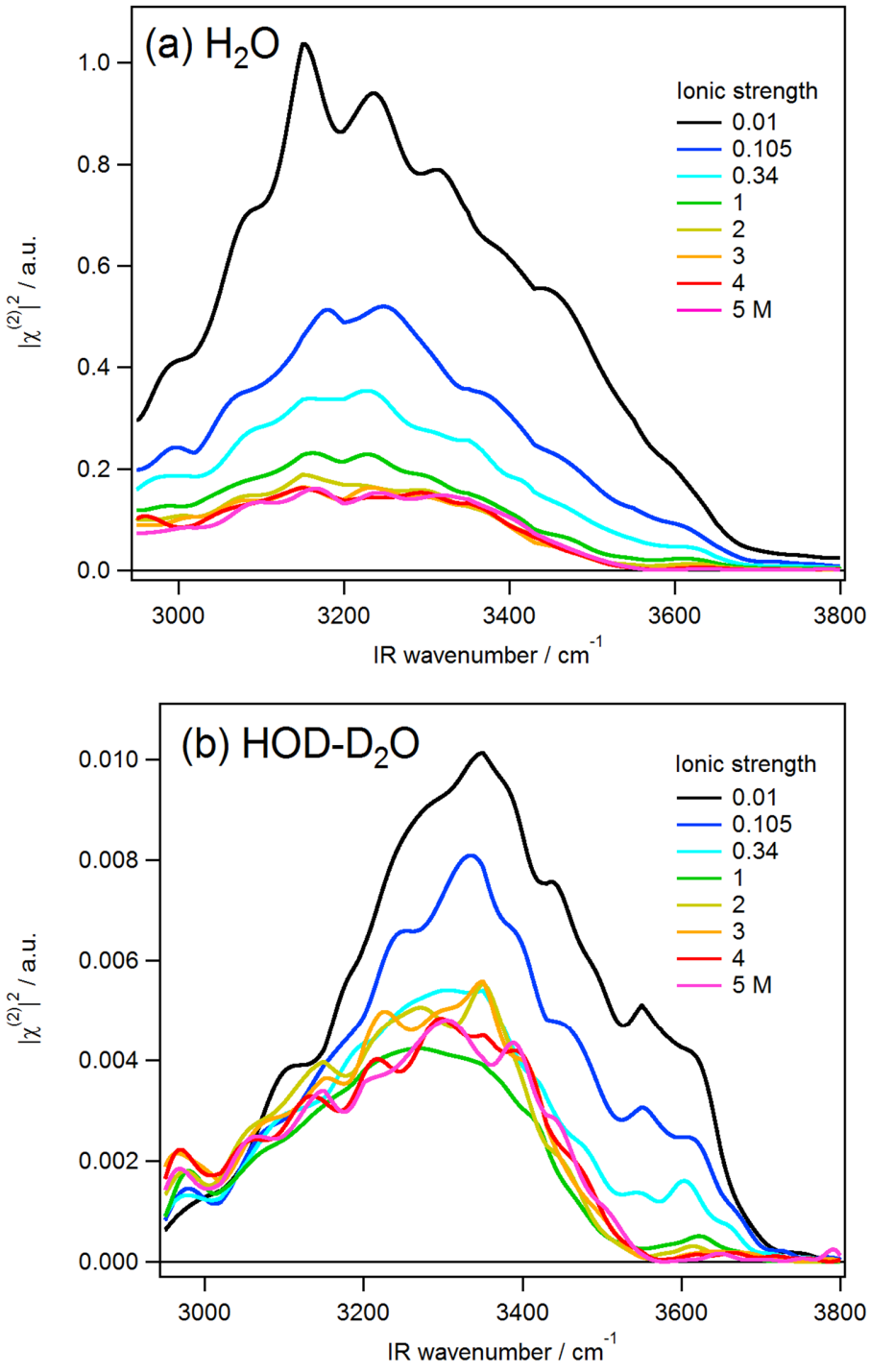

Figure S5. $|\chi^{(2)}|^2$ spectra reconstructed from the heterodyne-detected complex $\chi^{(2)}$ spectra. (a) H_2O, (b) HOD-D_2O solution.

References

(1) Myalitsin, A.; Urashima, S.; Nihonyanagi, S.; Yamaguchi, S.; Tahara, T., Water Structure at the Buried Silica/Aqueous Interface Studied by Heterodyne-Detected Vibrational Sum-Frequency Generation. *J. Phys. Chem. C* **2016**, *120*, 9357-9363.

(2) Glasoe, P. K.; Long, F. A., Use of Glass Electrodes to Measure Acidities in Deuterium Oxide. *J. Phys. Chem.* **1960**, *64*, 188-190.

(3) Krężel, A.; Bal, W., A Formula for Correlating pKa Values Determined in D_2O and H_2O. *J. Inorg. Biochem.* **2004**, *98*, 161-166.

(4) Nihonyanagi, S.; Yamaguchi, S.; Tahara, T., Direct Evidence for Orientational Flip-Flop of Water Molecules at Charged Interfaces: a Heterodyne-Detected Vibrational Sum Frequency Generation Study. *J. Chem. Phys.* **2009**, *130*, 204704.

(5) Sun, S.; Liang, R.; Xu, X.; Zhu, H.; Shen, Y. R.; Tian, C., Phase Reference in Phase-Sensitive Sum-Frequency Vibrational Spectroscopy. *J. Chem. Phys.* **2016**, *144*, 244711.

(6) Wen, Y.-C.; Zha, S.; Liu, X.; Yang, S.; Guo, P.; Shi, G.; Fang, H.; Shen, Y. R.; Tian, C., Unveiling Microscopic Structures of Charged Water Interfaces by Surface-Specific Vibrational Spectroscopy. *Phys. Rev. Lett.* **2016**, *116*, 016101.

(7) Ong, S.; Zhao, X.; Eisenthal, K. B., Polarization of Water Molecules at a Charged Interface: Second Harmonic Studies of the Silica/Water Interface. *Chem. Phys. Lett.* **1992**, *191*, 327-335.

(8) Wang, H.-F., Sum Frequency Generation Vibrational Spectroscopy (SFG-VS) for Complex Molecular Surfaces and Interfaces: Spectral Lineshape Measurement and Analysis Plus Some Controversial Issues. *Prog. Surf. Sci.* **2016**, *91*, 155-182.

(9) Joutsuka, T.; Hirano, T.; Sprik, M.; Morita, A., Effects of Third-Order Susceptibility in Sum Frequency Generation Spectra: a Molecular Dynamics Study in Liquid Water. *Phys. Chem. Chem. Phys.* **2018**, *20*, 3040-3053.

(10) Kilic, M. S.; Bazant, M. Z.; Ajdari, A., Steric Effects in the Dynamics of Electrolytes at Large Applied Voltages. I. Double-Layer Charging. *Phys. Rev. E* **2007**, *75*, 021502.

(11) Brown, M. A.; Goel, A.; Abbas, Z., Effect of Electrolyte Concentration on the Stern Layer Thickness at a Charged Interface. *Angew. Chem. Int. Ed.* **2016**, *55*, 3790-3794.

(12) Hasted, J. B.; Ritson, D. M.; Collie, C. H., Dielectric Properties of Aqueous Ionic Solutions. Parts I and II. *J. Chem. Phys.* **1948**, *16*, 1-21.

(13) Gavish, N.; Promislow, K., Dependence of the Dielectric Constant of Electrolyte Solutions on Ionic Concentration: A Microfield Approach. *Phys. Rev. E* **2016**, *94*, 012611.

(14) Nakayama, Y.; Andelman, D., Differential Capacitance of the Electric Double Layer: the Interplay Between Ion Finite Size and Dielectric Decrement. *J. Chem. Phys.* **2015**, *142*, 044706.

(15) Zhuang, X.; Miranda, P. B.; Kim, D.; Shen, Y. R., Mapping Molecular Orientation and Conformation at Interfaces by Surface Nonlinear Optics. *Phys. Rev. B* **1999**, *59*, 12632-12640.

(16) Leyendekkers, J. V.; Hunter, R. J., Refractive Index of Aqueous Electrolyte Solutions. Extrapolations to Other Temperatures, Pressures, and Wavelengths and to Multicomponent Systems. *J. Chem. Eng. Data* **1977**, *22*, 427-431.

(17) Querry, M. R.; Waring, R. C.; Holland, W. E.; Hale, G. M.; Nijm, W., Optical Constants in the Infrared for Aqueous Solutions of NaCl. *J. Opt. Soc. Am.* **1972**, *62*, 849-855.

(18) Max, J. J.; Chapados, C., Isotope Effects in Liquid Water by Infrared Spectroscopy. III. H_2O and D_2O Spectra from 6000 to 0 cm^{-1}. *J. Chem. Phys.* **2009**, *131*, 184505.

(19) Daimon, M.; Masumura, A., Measurement of the Refractive Index of Distilled Water from the Near-Infrared Region to the Ultraviolet Region. *Appl. Opt.* **2007**, *46*, 3811-3820.

(20) Malitson, I. H., Interspecimen Comparison of the Refractive Index of Fused Silica. *J. Opt. Soc. Am.* **1965**, *55*, 1205-1209.